Mass Diffusion and Thermal Diffusivity of the Decane-pentane Mixture Under High Pressure as a Ground-based Study for SCCO Project

I. Lizarraga, C. Giraudet, Fabrizio Croccolo, M.M. Bou-Ali, Henri Bataller

1 # Mass diffusion and thermal diffusivity of the decane-pentane

2 # mixture under high pressure as a ground-based study for SCCO

3 # project

4 Ion Lizarraga[1], Cédric Giraudet[2], Fabrizio Croccolo[2], M. Mounir Bou-Ali[1], and Henri

5 Bataller[2]

6 *[1] MGEP Mondragon Goi Eskola Politeknikoa, Mechanical and Industrial Manufacturing*

7 *Department, Loramendi 4 Apdo. 23, 20500 Mondragon, Spain*

8 *[2] Laboratoire des Fluides Complexes et leurs Réservoirs, UMR-5150, Université de Pau et*

9 *des Pays de l'Adour, 1 Allée du Parc Montaury, Anglet, FR.*

10

11 **Abstract**

12 Thermodiffusion experiments on iso-massic binary mixture of decane and pentane in the

13 liquid phase have been performed between 25°C and 50°C and for pressures from 1MPa until

14 20MPa. By dynamic analysis of the light scattered by concentration non-equilibrium

15 fluctuations in the binary mixture we obtained the mass diffusion coefficients of the mixture

16 at each temperature and pressure. For the first time we were able to apply similar analysis to

17 thermal fluctuations thus getting a simultaneous measurement of the thermal diffusivity

18 coefficient. While mass diffusion coefficients decrease linearly with the pressure, thermal

19 diffusivity coefficients increase linearly. In principle the proposed method can be used also

20 for measuring the Soret coefficients at the same time. However, for the present mixture the

21 intensity of the optical signal is limited by the optical contrast factor. This affects our

22 capability of providing a reliable estimate of the Soret coefficient by means of dynamic

23 Shadowgraph. Therefore the mass diffusion coefficients measurements would need to be

24 combined with independent measurements of the thermodiffusion coefficients, e.g.

25 thermogravitational column, to provide Soret coefficients. The obtained values constitute the

on-ground reference measurements for one of the mixture studied in the frame of the project SCCO-SJ10, which aims to measure the Soret coefficients of multicomponents mixtures under reservoir conditions. Microgravity experiments will be performed on the Chinese satellite SJ10 launched in April 2016.

1.   Introduction

The precise modelling of the distribution of chemical species in oil and gas reservoirs remains a topical issue for the oil industry, especially now that the reserves of fossil fuels are getting more difficult to extract. It is known that not only gravitational segregation, but also thermodiffusion due to geothermal gradients, are two physical phenomena determining the vertical distribution of species in hydrocarbon reservoirs on Earth (Lira-Galeana et al. 1994, Høier et al. 2001, Ghorayeb et al. 2003, Montel et al. 2007). Thermodiffusion, or Soret effect, is a phenomenon that couples heat and mass fluxes (de Groot and Mazur 1984) and can also lead to convective unstable conditions in particular cases (Galliero et al. 2009). The contribution of thermodiffusion is difficult to quantify, mainly due to a lack of experimental data as well as accurate modeling for multicomponent mixtures. Although noticeable progresses have been made during the last twenty years, (Assael et al., 2014 and references therein) especially on ternary mixtures both theoretically (Firoozabadi et al., 2000; Kempers, 2001; Galliero et al., 2003) and experimentally (Leahy-Dios et al., 2005; Larrañaga et al., 2015; Gebhardt et al., 2015), more work is necessary. Micro-gravity experiments, to avoid gravity-induced convection, are one possible way to provide further data on thermodiffusion in multicomponent mixtures (Georis et al., 1998; Van Vaerenbergh et al., 2009; Touzet et al., 2011; Bou-Ali et al., 2015). The Soret Coefficients in Crude Oil (SCCO) project aims at producing values of Soret coefficients of mixture of petroleum interest and in reservoirs conditions. In a first phase carried out in 2007 microgravity experiments were performed on board the Russian satellite FOTON-M3. One binary, two ternaries and one quaternary mixtures were studied (Van Vaerenbergh et al., 2009; Srinivasan et al., 2009; Touzet et al., 2011). The measurements were compared with molecular dynamics simulations and with theoretical calculations based on the Thermodynamics of Irreversible Processes. However, the conclusions were incomplete because of difficulties encountered during post flight analysis at

58   the laboratories (Touzet et al., 2011). Now, on the occasion of the China Sea well

59   explorations, a second phase of the SCCO space experiment has been scheduled. The

60   thermodiffusion behaviour of the binary mixture decane-pentane, the ternary mixture decane-

61   heptane-pentane and the quaternary mixture decane-heptane-pentane-methane, at two

62   pressures and at 50°C, will be studied on-board the Shijian-10 (SJ-10) Chinese satellite during

63   2016 (Galliero et al., 2015). To assure the success of this new mission, both validating ground

64   measurements and numerical simulations have been planned. In this paper we present results

65   on the iso-massic binary mixture decane-pentane based on the measurement of non-

66   equilibrium (NE) fluctuations.

67   In general, from the analysis of the dynamics of concentration NE fluctuations by light-

68   scattering it is possible to measure the fluid transport properties coefficients, including the

69   mass diffusion and Soret coefficients, as demonstrated for binary mixtures (Croccolo et al.,

70   2012, 2014). The technique has been adapted to high pressure (Giraudet et al., 2014). In this

71   work we extend the technique to the analysis of thermal fluctuations thus including the

72   possibility of measuring the thermal diffusivity coefficient of the mixture. Conversely, due to

73   the limited amplitude of the optical signal obtained for this system, we were not able here to

74   measure the Soret coefficient.

75   The remainder of the paper is organized as follows: Section 2 reports the methodology, in

76   Section 3 we provide results and discussion, and in Section 4 conclusions are drawn.

77

78   **2.   Methodology**

79

80   *Theoretical background*

81   In a homogeneous multicomponent mixture a temperature gradient induces heat transfer as

82   well as segregation of the components along the temperature gradient by means of the Soret

83   effect (de Groot and Mazur, 1984). The segregation induces then Fickean diffusion and the

84   combination of the two phenomena results in a steady concentration gradient which is

85   convection-free only in microgravity conditions or in particular cases on ground. A

86   thermodiffusion experiment on ground is typically performed by applying a stabilizing

87   thermal gradient to a multicomponent fluid mixture, thus obtaining a superposition of the

88   mentioned phenomena. Even if there is no total mass flux in the steady state, thermal and

89   concentration NE fluctuations are always present. NE fluctuations are strictly related to the

90   transport properties of the fluid. That is why from NE fluctuations analysis one can determine

91   in principle all transport coefficients, like viscosity, thermal diffusivity and solutal diffusion

92   and thermodiffusion coefficients. A detailed description of the theory of NE fluctuations can

93   be found in the book by Ortiz de Zárate and Sengers (Ortiz de Zárate and Sengers, 2006).

94   Here we briefly recall the essential equations that will be used in the following.

95   In a binary mixture, the temporal correlation function of NE concentration fluctuations

96   induced by the Soret effect is expected to be a single exponential decay for all wave vectors,

97   with time constants $\tau_S(q)$ varying as a function of the wave vector q. For wave vectors much

98   larger than a characteristic value q_s^*, the decay time is the solutal diffusive one:

99

100          $\tau_S(q) = 1/(Dq^2)$,   (Eq. 1)

101

102   where D is the mass diffusion coefficient. NE thermal fluctuations are faster and overlap to

103   the solutal ones. For wave vectors larger than a thermal characteristic wave vector q_T^*, the

104   decay time is the thermal diffusive one:

105

106          $\tau_T(q) = 1/(\kappa q^2)$,   (Eq. 2)

107

108   where κ is the thermal diffusivity coefficient.

109

110   *Experimental set-up*

111   Our thermodiffusion cell (Fig.1 of Giraudet et al., 2014) is specifically designed for applying

112   a vertical temperature gradient with excellent thermal homogeneity and stability to a

113   horizontal slab of a multicomponent fluid under high pressure while providing vertical optical

114   access to a central area of the cell. The cell core consists of a stainless steel annulus of

115   internal/external diameter 30/75mm with high pressure inlet and outlet at its opposite sides.

116   This part accommodates Teflon®-coated Viton® O-rings for sealing, and square sapphire

117   plates kept at a distance L = 5mm by the annulus itself, thus defining the sample thickness. In

118   order to minimize the contact between the liquid sample and the conductive metal a Teflon

119   annulus (internal/external diameter 19.8/30mm) with two thin holes (diameter 1mm) for

120   inlet/outlet of the fluid has been inserted in the inner part of the stainless annulus zone.

121   The external sides of the sapphire windows are in thermal contact with two aluminium plates

122   with a central circular aperture (d=13mm), where two thermistors (Wavelenght Electronics,

123   TCS651) are installed to monitor the sapphire temperatures. External to the aluminium plates,

124   two Peltier elements (Kryotherm, TB-109-1.4-1.5 CH) with central circular aperture

125   (d=13mm) provide/remove the heat necessary to maintain the set-point temperature as driven

126   by two temperature controllers (Wavelenght Electronics, LFI-3751) maintaining the

127   temperature of the internal side of each Peltier device with a stability better than 1mK RMS

128   over 1 day. Finally, external to the Peltier elements, two aluminium plates are flushed with

129   water coming from a thermostatic bath (Huber, ministat 125) to remove the excess heat of the

130   Peltiers.

131   Experiments have been performed with the iso-massic binary mixture of decane (Sigma-

132   Aldrich, ≥99%) and pentane (Sigma-Aldrich, ≥99%). Components were used without further

133   purification. The mixture is prepared in a bottle by weighting on a balance (Sartorius,

134   TE313S, resolution 10^{-2}g/200g) first the decane and then the pentane. The bottle is carefully

135   closed by cover with Teflon sealing. Error in mass fraction is estimated less than ±0.0001.

136   The filling system consists of: a rotary vacuum pump able to evacuate most of the air from the

137   cell before filling operations down to a residual pressure of about 10Pa; a fluid vessel at

138   atmospheric pressure; a manual volumetric pump and a number of valves to facilitate the

139   procedure. Briefly, after a low vacuum is made inside the cell, the mixture to be studied is

140   transferred to the cell by acting on the volumetric pump. Visual check allows avoiding

141   bubbles during the injection procedure. After that, the cell is abundantly fluxed with the fluid

142   mixture. At the end of the procedure a valve is closed and the volumetric pump is operated to

143   modify the liquid pressure within the cell. A manometer (Keller, PAA-33X, pressure range:

144   0.1÷100MPa, precision ±0.04MPa) is connected between the volumetric pump and the cell to

145   measure the pressure of the fluid mixture. A second identical manometer is connected to the

146   outlet of the cell. The manometer signals are transferred using an acquisition card (National

147   Instruments, NI 9215) interfaced to a computer.

148   We perform our experiments by imposing a difference of temperature ΔT on the horizontally

149   positioned thin cell, previously filled with the homogenous fluid mixture.

150   In order to investigate NE fluctuations, it is common to use a scattering in the near field

151   technique as the Shadowgraph (Wu et al. 1995), for which the physical optics treatment was

152   given by Trainoff and Cannell (2002) and Croccolo and Brogioli (2011). The shadowgraph

153   optical setup involves a low coherence light source (Super Lumen, SLD-MS-261-MP2-SM, λ

154   = 675±13nm) that illuminates the bottom of the cell through a single-mode fiber. The

155   diverging beam exiting from the fiber end is collimated by an achromatic doublet lens (f =

156   150mm, φ=50.8mm) and then passes through a linear film polarizer. In combination with a

157   second linear polarizer after the cell the latter allows us to adapt the average light intensity.

158   The detection plane is located at about $z = 95mm$ from the sample plane. As a sensor, we use

159   a charge coupled device (AVT, PIKE-F421B) with 2048 ×2048 square pixels each of size 7.4

160   ×7.4μm^2 and a dynamic range of 14-bit. Images were cropped within a 768x768pix^2 in order

161   to reach the maximum acquisition frame rate of the camera of about 30Hz.

162

163   ***Dynamic near-field imaging***

164   Images acquired by means of a near-field scattering setup consist of an intensity map $I(\vec{x},t)$

165   generated by the interference on the CCD plane between the portion of the incident beam that

166   has passed undisturbed through the sample and the beams scattered by refractive index

167   fluctuations occurring within the sample (Trainoff and Cannell, 2002; Croccolo and Brogioli,

168   2011). Statistical analysis involving fast Fourier transforms provides accurate measurements

169   of the intensity $I_s(\vec{q},t)$ of light scattered at each wave vector $\vec{q}$ grabbed by the optical setup

170   and for all the times t of the acquisition sequence. Different setups show different responses to

171   the acquired signal as a function of the wave number q, which is described by the so-called

172   transfer function $T(q)$.

173

174

175   *(a)*   *(b)*   *(c)*
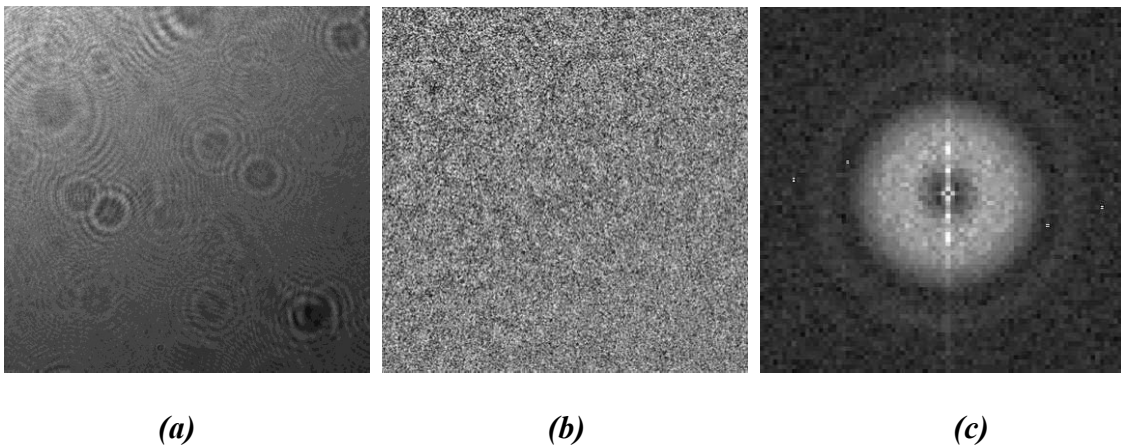
176   ***Figure 1***: *Results of a near field scattering experiment (shadowgraph layout) on the iso-*

177   *massic binary of decane and pentane stressed by a thermal gradient ($T_{mean} = 50°C$, $P = 20$*

178   *MPa, ΔT = 30°C).(a) 768×768 pix^2 near field image of the sample, $I(\vec{x},t)$ (b) image*

179   *difference, $\Delta I(\vec{x},\Delta t) = I(\vec{x},t+\Delta t) - I(\vec{x},t)$, having a correlation time of Δt =0.35 s and (c)*

180   *2D Fast Fourier Transform squared $\left| I(\vec{q},t+\Delta t) - I(\vec{q},t) \right|^2$ of (b).*

181

182   Details of the quantitative dynamic analysis can be found elsewhere (Croccolo et al., 2006a;

183   Croccolo et al., 2006b; Croccolo et al., 2007; Cerchiari et al., 2012). Here we just recall that

184   the quantity directly obtained from the experiments is the so-called structure function

185    $C_m(q,\Delta t) = \left\langle \left| \Delta I_m(q,\Delta t) \right|^2 \right\rangle$, that is obtained by averaging (over all available times t in each

186   image dataset and over the wave vector $\vec{q}$ azimuthal angle) the individual spatial Fourier

187   transforms of the shadowgraph image differences, like the one shown in the example of Fig.

188   1. This experimental structure function is theoretically related to the temporal correlation

189   function of NE composition fluctuations, also called intermediate scattering function (*ISF*),

190   by:

191

192    $$C_m(q,\Delta t) = 2\{S(q)T(q)[1 - ISF(q,\Delta t)] + B(q)\}, \qquad \text{(Eq.3)}$$

193

194   with $ISF(q,0) = 1$. In Eq.3, $S(q)$ is the static power spectrum of the sample, $T(q)$ is the optical

195   transfer function and $B(q)$ the background noise of the measurement. It is implicitly assumed

196   in Eq.3 that the linear response of the CCD detector and any other electronic or

197   electromagnetic proportionality parameters are aggregated inside $T(q)$ and/or $B(q)$.

198

199   **3.   Results and Discussion**

200

201   ***Thermodynamic conditions***

9

202   To determine the thermodynamic conditions of the study, we have calculated, with TOTAL

203   S.A. company BEST software, the biphasic envelop and critical coordinates of the iso-massic

204   binary mixture of decane and pentane. For a given pressure P and a given temperature T, the

205   software calculates the possible molar volumes v from the PPR78 equation of state (Peng and

206   Robinson, 1976). In Fig.2 we report the calculated biphasic envelop.

207
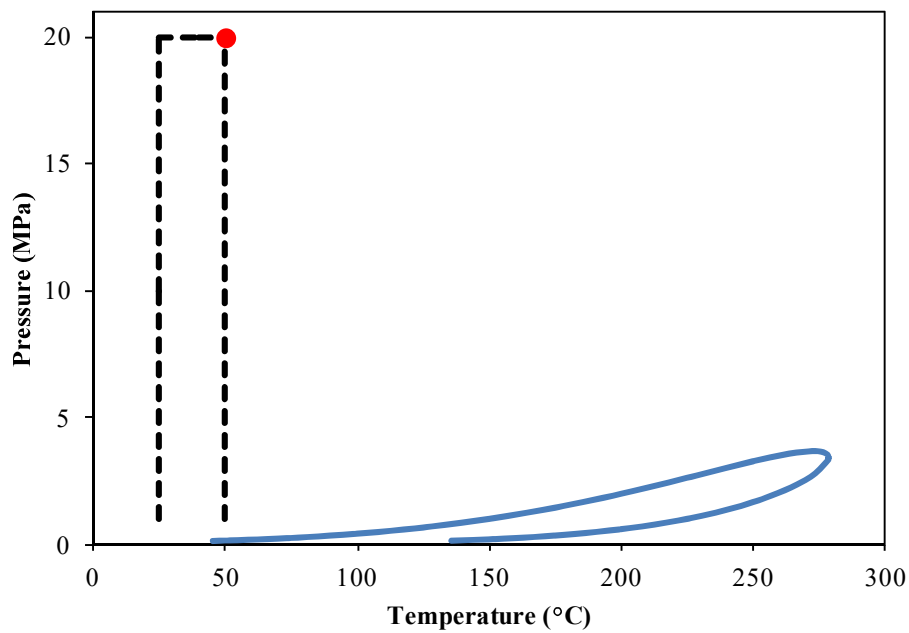
208

209   ***Figure 2****: Phase diagram of the isomassic binary mixture decane-pentane: the continuous*

210   *line represents the biphasic envelop. The dashed lines represent the values of pressure and*

211   *temperature investigated for the reported thermodiffusion experiments. The red point*

212   *indicates the thermodynamic conditions of the thermodiffusion experiment shown in Fig. 1, 3*

213   *and 4 (T_{mean} = 50°C, P = 20 MPa).*

214

215   In Fig.2 the dashed line represents the values of pressure and temperature investigated for

216   the present thermodiffusion experiments, the temperature of 50°C being imposed by the

217   microgravity experimental conditions of the SCCO project, and the temperature of 25°C

218   being selected as the experimental data references for mass diffusion coefficients only exist at

219 this temperature. Initially, a temperature difference of 20°C was applied to the system. To

220 increase the optical signal, which remains low as revealed by Fig.1b-c, we applied a

221 temperature difference of 30°C. In all the investigated conditions the mixture was in its liquid

222 state, even at low pressure and for temperature differences of $\Delta T = 20$ and 30°C. The red

223 point in Fig.2 indicates the thermodynamic conditions of the thermodiffusion experiment

224 shown in Fig.1, 3 and 4 ($T_{\mathrm{mean}} = 50$°C, $P = 20$ MPa).

225

226 ***Structure function***

227 At each investigated temperature T and pressure P, 10 different image acquisition runs have

228 been performed with a delay time $dt_{\mathrm{min}} = 35$ms between two consecutive images. Each set,

229 containing 2000 images, has then been processed on a dedicated PC by means of a custom-

230 made CUDA/C++ software (Cerchiari et al., 2012), in order to perform a fast parallel

231 processing of the images to obtain the structure functions $C_m(q, \Delta t)$, for all the wave numbers

232 and for all the correlation times accessible within the image datasets. In each experiment the

233 temperature gradient is applied via two distinct temperature controllers, so that a linear

234 temperature gradient sets up in some tens of seconds. The image acquisition is started about

235 five hours later, to be sure that the concentration gradient due to the Soret effect is fully

236 developed within the cell.

237 In Fig.3 we present the mean structure function $C_m(q, \Delta t)$ of the 10 runs a) as a function of the

238 wave number for different correlation times and b) as a function of the correlation time for

239 different wave numbers, for mean temperature $T_{\mathrm{mean}} = 50$°C, pressure $P = 20$MPa and a

240 difference of temperature $\Delta T = 30$°C. The oscillatory behavior shown in Fig.3a is due to the

241 optical transfer function $T(q)$ (see Eq.3). It is typical of shadowgraph experiments and it

242 corresponds to the ring pattern shown in Fig. 1c.

243

244

245   (a)   (b)
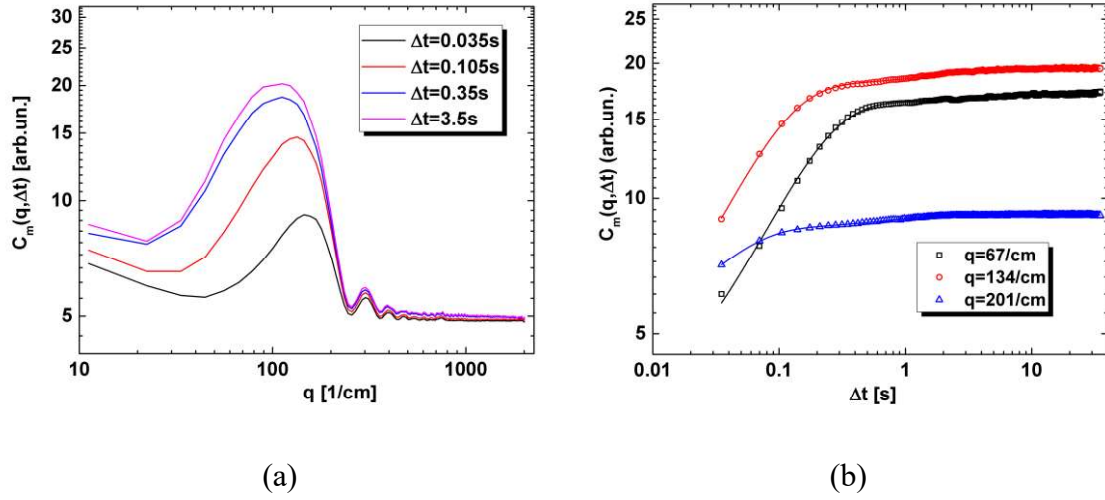
246   **Figure 3**: *Experimental structure function* $C_m(q, \Delta t)$ *(a) as a function of the wave vector q for*

247   *different correlation times* Δt *and (b) as a function of the correlation time* Δt *for different*

248   *wave vectors q* ($T_{mean} = 50°C$, $P = 20MPa$, $\Delta T = 30°C$).

249

250   Fig.3a shows that for wave numbers $q > 400cm^{-1}$, the signal is completely lost in the

251   background noise. For intermediate wave numbers, Fig.3b shows that the time dependence of

252   the structure function cannot be totally assumed mono-exponential, as it is visible for wave

253   numbers $q = 134cm^{-1}$ and $201cm^{-1}$. To account for the solutal relaxation mode plus the

254   thermal relaxation mode, we therefore decided to perform a quantitative analysis of the

255   experimental structure functions by modeling the *ISF* as a double exponential decay, namely:

256

257     $$ISF(q, \Delta t) = a \exp\left(-\frac{\Delta t}{\tau_1(q)}\right) + (1-a) \exp\left(-\frac{\Delta t}{\tau_2(q)}\right), \qquad \text{(Eq. 4)}$$

258

259   where τ_1 and τ_2 are two relaxation times. Hence, we performed fittings of the experimental

260     $C_m(q, \Delta t)$ as a function of Δt (see Fig.3b) by substituting Eq.4 into Eq.3 and adopting as fitting

261   parameters: the product $S(q)T(q)$, the background $B(q)$, the relative amplitude a, and the two

262   decay times, τ_1 and τ_2. For the fitting procedure we used a Levenberg-Marquardt Non-Linear

263   Least Square fitting algorithm.

264
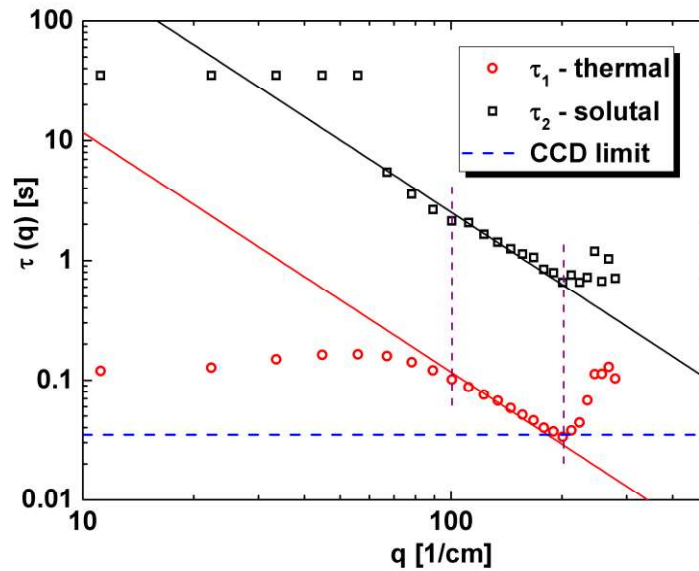
265

266   **Figure 4**: *Experimental decay times of NE fluctuations as obtained by fitting through Eqs.3*

267   *and 4, as a function of the wave number q. $\bigcirc$: fast mode, $\square$: slow mode (T_{mean} = 50°C, P =*

268   *20MPa, ΔT = 30°C). The black solid line represents the theoretical relaxation times $1/Dq^2$ of*

269   *Eq.1 and the red solid line represents the theoretical relaxation times $1/\kappa q^2$ of Eq.2.*

270

271   In Fig.4 we show the two decay times obtained from modeling the *ISF* by Eq.4, as a function

272   of the wave number. The horizontal dashed blue line corresponds to dt_{min} = 35ms, which is

273   the physical limit of our experimental recording equipment.

274   Intuitively, we assumed that the fastest mode was associated with a thermal mode and the

275   slowest to a solutal mode.

276   In the range of wave numbers $100\,cm^{-1} \leq q \leq 200\,cm^{-1}$ (vertical dotted lines are plotted in Fig.4

277   to guide the reader) the slowest mode was fitted with Eq.1 using D as free parameter and the

278 fastest was fitted with Eq.2 using κ as free parameter. The results of the adjustments are

279 reported by continuous lines in Fig.4. For example, referring to the conditions of Fig.4 (P =

280 20MPa, T_{mean} = 50°C) the two values obtained by fitting are D = (38±4)x10^{-6}cm^2/s and κ =

281 (870±40)x10^{-6}cm^2/s. Uncertainties are the average of the deviations respect to the mean value

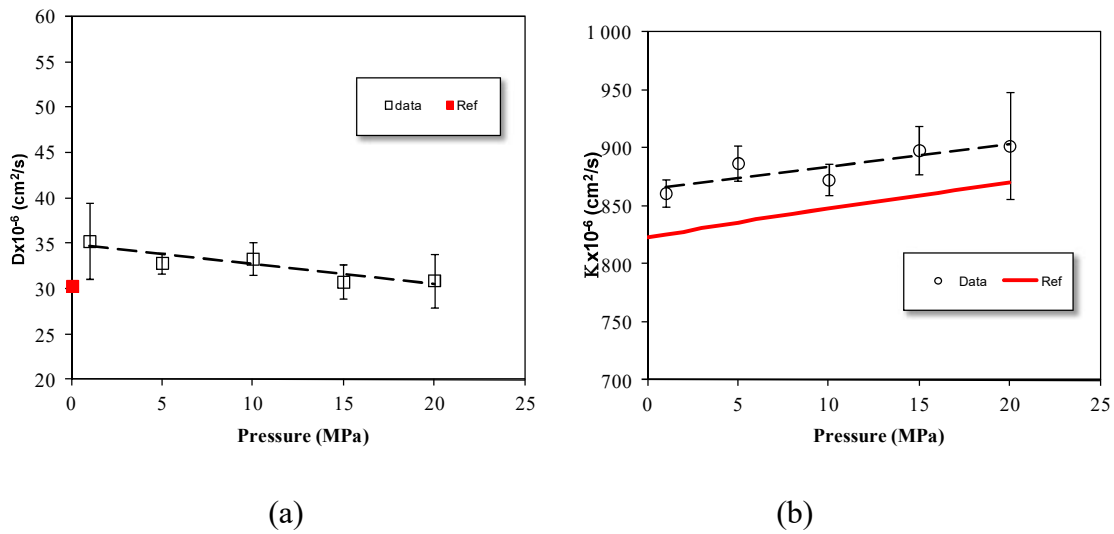282 of the 10 measurements.

283

284 ***Mass diffusion and thermal diffusivity coefficients***

285

286 In Fig.5 we report the values of mass diffusion and thermal diffusivity coefficients as a

287 function of the pressure obtained for the iso-massic binary mixture of decane and pentane, at

288 T_{mean} = 25°C and for a temperature difference ΔT = 20°C.

289

290

291   (a)   (b)

292 **Figure 5:** *Mass diffusion D and thermal diffusivity κ coefficients as a function of the pressure*

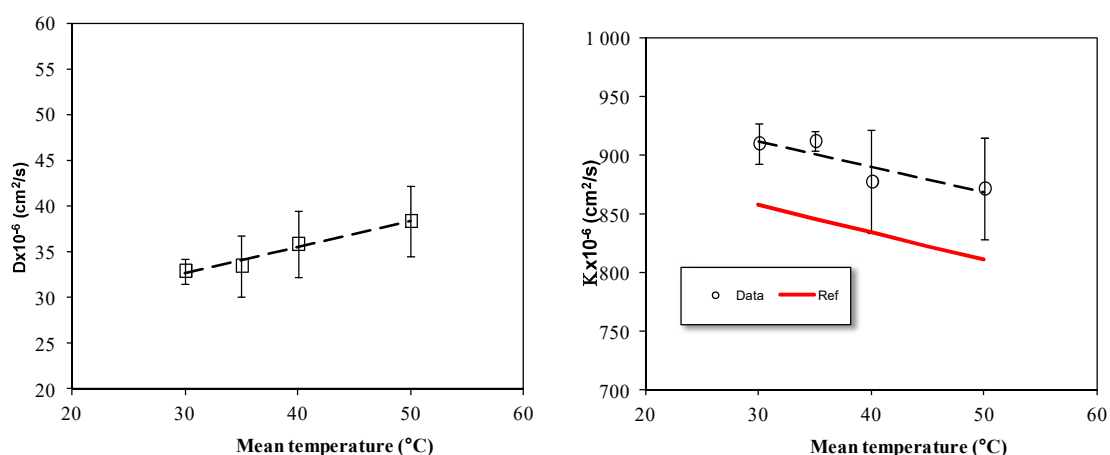293 *at T_{mean}= 25°C and for a temperature difference of ΔT = 20°C.*

294

295 We found only one reference value of the mass diffusion coefficients at atmospheric pressure

296 (Alonso De Mezquia et al., 2012) that we reported in Fig.5a as a red point. The thermal

297   diffusivity coefficients were compared with values found in NIST data base (NIST website)

298   and reported by a red continuous line in Fig.5b. Our values slightly overestimate reference

299   values. However, over the entire pressure range studied, the relative deviation of the thermal

300   diffusivity coefficients values does not exceed 5%. These results validate our hypothesis for

301   the interpretation of the modes of the measured intermediate scattering function, namely that

302   the fastest mode is the thermal relaxation mode of NE fluctuations and the slowest a mass

303   relaxation mode.

304   In Fig.5a we can notice a slight linear decrease in the mass diffusion coefficient with pressure

305   that is consistent with an increase of the viscosity with pressure (mass diffusion coefficient

306   being proportional to the inverse of the viscosity), as it has been shown in Alonso De Mezquia

307   et al., 2012. Also in Fig.5b we can see a linear increase in the thermal diffusivity coefficients

308   with pressure that is consistent with an increase of the density with pressure.

309   In Figure 6 we report the values of mass diffusion and thermal diffusivity coefficients as a

310   function of the mean temperature obtained for the iso-massic binary mixture of decane and

311   pentane, at $P = 20$MPa and for a temperature difference $\Delta T = 30°C$.

312

313

314   (a)   (b)

315   ***Figure 6:*** *Mass diffusion D and thermal diffusivity κ coefficients as a function of the mean*

316   *temperature at P= 20MPa and for a temperature difference of ΔT = 30°C.*

317

318   In Fig.6a we can see that the mass diffusion coefficient increases with the mean temperature,

319   which is consistent with a decrease of the viscosity of the system with the mean temperature.

320   In Fig.6b we can see that the thermal diffusivity coefficient decreases with the mean

321   temperature. Again an overestimate of the reference values is detected.

322   In Fig.7 we report the values of mass diffusion and thermal diffusivity coefficients as a

323   function of the pressure obtained for the iso-massic binary mixture of decane and pentane, at

324   T_{mean} = 50°C and for a temperature difference $ΔT$ = 30°C. The same trends as for Fig.5 are

325   observed.

326
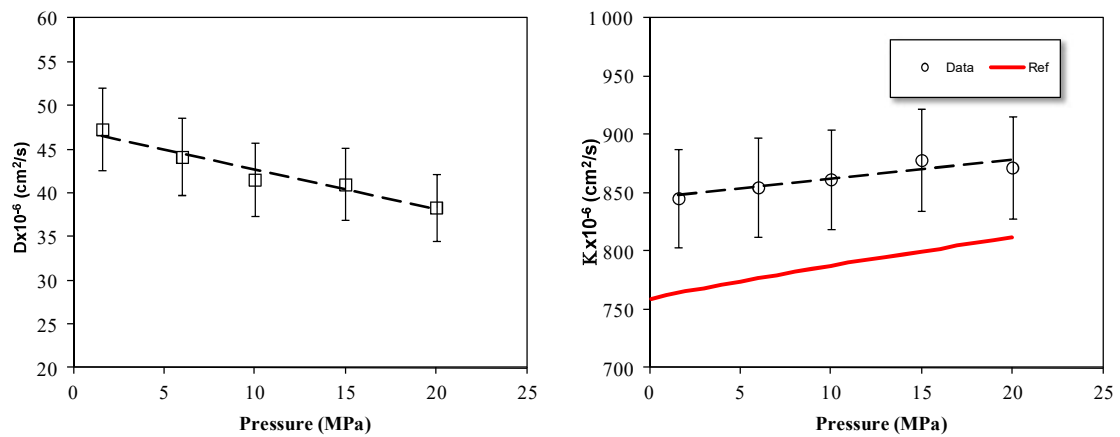
327

328   ***Figure 7:*** *Mass diffusion D and thermal diffusivity κ coefficients as a function of the pressure*

329   *at T_{mean}= 50°C and for a temperature difference of ΔT = 30°C.*

330

331   **4.   Conclusions**

332

333 Thermodiffusion experiments on iso-massic binary mixture of decane and pentane, in the

334 liquid phase, have been performed between 25°C and 50°C and for pressures from 1MPa until

335 20MPa. By means of dynamic analysis of the light scattered by concentration NE fluctuations

336 of the binary mixture we obtained the values of the mass diffusion coefficient D at each

337 temperature and pressure. The shadowgraph set-up and its acquisition chain enabled us to

338 achieve a minimum delay time between two successive images of 35ms. We were thus able to

339 investigate for the first time temperature NE fluctuations, which let us model the ISF as the

340 sum of two decreasing exponentials. This procedure allowed obtaining simultaneously the

341 values of the thermal diffusivity coefficient κ. Mass diffusion coefficients D decrease with the

342 pressure while thermal diffusivity coefficients κ increase with the pressure. For the

343 investigated mixture, due to a limited intensity of the optical signal, it was not possible to

344 obtain a reliable measurement of the Soret coefficients S_T. Therefore the obtained values of

345 the mass diffusion coefficients D must be combined with thermodiffusion coefficients D_T

346 measurements obtained by an independent experiment, such as thermogravitational column.

347 The resulting values at 50°C can be directly compared to measurements made in microgravity

348 in the frame of the SCCO-SJ10 project.

349

350

356

357 **References**

358   - Alonso de Mesquia, D., Bou-Ali, M.M., Larrañage, M., Madariaga, J.A., Santamaria,

359   C.: Determination of molecular diffusion coefficient in n-alkane binary mixtures:

360   Empirical correlations. J. Phys. Chem. B 116, 2814-2819 (2012).

361   - Assael, M.J., Goodwin, A.R.H., Vesovic, V., Wakeham, W.A.: Experimental

362   Thermodynamics Volume IX: Advances in Transport Properties of Fluids, Royal

363   Society of Chemistry, London, (2014).

364   - Bou-Ali, M.M., Ahadi, A., Alonso de Mezquia, D., Galand, Q., Gebhardt, M., Khlybov,

365   O., Köhler, W., Larrañaga, M., Legros, J.C., Lyubimova, T., Mialdun, A., Ryzhkov, I.,

366   Saghir, M.Z., Shevtsova, V., Van Vaerenbergh, S.: Benchmark values for the Soret,

367   thermodiffusion and molecular diffusion coefficients of the ternary mixture

368   tetralin+isobutylbenzene+n-dodecane with 0.8-0.1-0.1 mass fraction. Eur. Phys. J. E

369   38, 30 (2015).

370   - Cerchiari, G., Croccolo, F., Cardinaux, F., Scheffold, F.: Quasi-real-time analysis of

371   dynamic near field scattering data using a graphics processing unit. Rev. Sci. Instrum.

372   83, 106101 (2012).

373   - Croccolo, F., Brogioli, D., Vailati, A., Giglio, M., Cannell, D.S.: Use of the dynamic

374   Schlieren to study fluctuations during free diffusion. App. Opt. 45, 2166-2173

375   (2006a).

376   - Croccolo, F., Brogioli, D., Vailati, A., Giglio, M., Cannell, D.S.: Effect of gravity on the

377   dynamics of non equilibrium fluctuations in a free diffusion experiment. Ann. N. Y.

378   Acad. Sci. 1077, 365 (2006b).

379   - Croccolo, F., Brogioli, D., Vailati, A., Giglio, M., Cannell, D.S.: Non-diffusive decay of

380   gradient driven fluctuations in a free-diffusion process. Phys. Rev. E. 76, 41112

381   (2007).

382   - Croccolo, F., Brogioli, D.: Quantitative Fourier analysis of schlieren masks: the

383   transition from shadowgraph to schlieren. App. Opt. 50, 3419-3427 (2011).

384   - Croccolo, F., Bataller, H., Scheffold, F.: A light scattering study of non equilibrium

385   fluctuations in liquid mixtures to measure the Soret and mass diffusion coefficient. J.

386   Chem. Phys. 137, 234202 (2012).

387   - Croccolo, F., Bataller, H., Scheffold, F.: Static versus dynamic analysis of the influence

388   of gravity on concentration non equilibrium fluctuations. Eur. Phys. J. E 37, 105

389   (2014).

390   - de Groot, S.R., Mazur, P: *Nonequilibrium Thermodynamics*. Dover, New York (1984).

391   - Firoozabadi, A., Ghorayeb, K., Shukla, K.: Theoretical model of thermal diffusion

392   factors in multicomponent mixtures, AIChE Journal 46, 892-900, 2000.

393   - Galliero, G., Duguay, B., Caltagirone, J.P., Montel, F.: On thermal diffusion in binary

394   and ternary mixtures by non-equilibrium molecular dynamics, Phil. Mag. 83, 2097-

395   2108 (2003).

396   - Galliero, G., Montel, F.: Understanding compositional grading in petroleum reservoirs

397   thanks to molecular simulations. Society of Petroleum Engineers Paper. 121902,

398   Amsterdam, 2009

399   - Galliero, G., Bataller, H., Croccolo, F., Vermorel, R., Artola, P.-A., Rousseau, B.,

400   Vesovic, V., Bou-Ali, M., Ortiz de Zárate, J.M., Xu, S., Zhang, K., Montel, F.: Impact

401   of Thermodiffusion on the initial distribution of Species in hydrocarbon reservoirs.

402   Microgravity Sci. Technol. DOI 10.1007/s12217-015-9465-6.

403   - Gebhardt M. and Köhler W.: Soret, thermodiffusion, and mean diffusion coefficients of

404   the ternary mixture ndodecane+ isobutylbenzene+1,2,3,4 tetrahydronaphthalene. J.

405   Chem. Phys. 143, 164511 (2015).

406   - Georis, P., Montel, F., Van Vaerenbergh, S., Decoly, Y., Legros, J.C.: Proceedings of

407   the European Petroleum Conference, 1, pp. 57-62 (1998).

408   - Ghorayeb, K., Firoozabadi, A., Anraku, T.: Interpretation on the unusual fluid

409   distribution in the Yufutsu gas-condensate field. SPE J. 8, 114-123 (2003).

410   - Giraudet, C., Bataller, H., Croccolo, F.: High-pressure mass transport properties

411   measured by dynamic near-field scattering of non-equilibrium fluctuations. Eur. Phys.

412   J. E 37, 107 (2014).

413   - Høier, L., Whitson, C.H.: Compositional grading-theory and Practice. SPE Reserv.

414   Evaluation Eng. 4, 525-532 (2001).

415   - Kempers L.J.T.M.: A comprehensive thermodynamic theory of the Soret effect in a

416   multicomponent gas, liquid, or solid, J. Chem. Phys. 115, 6330-6341 (2001).

417   - Larrañaga M., Bou-Ali M., Lizarraga I., Madariaga J.A., Santamaría S.: Soret

418   Coefficients of the Ternary Mixture 1,2,3,4-Tetrahydronaphthalene + Isobutylbenzene

419   + N-Dodecane, J. Chem. Phys. 143, 024202 (2015).

420   - Leahy-Dios, A., Bou-Ali, M.M., Platten, J.K., Firoozabadi, A.: Measurements of

421   molecular and thermal diffusion coefficients in ternary mixtures, J. Chem. Phys. 122,

422   234502 (2005).

423   - Lira-Galeana, C., Firoozabadi, A., Prausnitz, J.M.: Computation of compositional

424   grading in hydrocarbon reservoirs. Application of continuous thermodynamics. Fluid

425   Phase Equilib. 102, 143-158 (1994).

426   - Montel, F., Bickert, J., Lagisquet, A., Galliero, G.: Initial state of petroleum reservoirs:

427   A comprehensive approach. J. Pet. Sci. Eng. 58, 391-402 (2007).

428   - NIST website: http://webbook.nist.gov/chemistry/

429   - Ortiz de Zárate J.M., Sengers, J.V.: Hydrodynamic Fluctuations in Fluids and Fluid

430   Mixtures, Elsevier, Amsterdam, (2006).

431   - Peng, D.Y., Robinson, D.B.: A new two-constant equation of state. Ind. Eng. Chem.

432   Fundam. 15, 59-64 (1976).

433   - Srinivasan, S., Saghir, M.Z.: Measurements on thermodiffusion in ternary hydrocarbon

434   mixtures at high pressure. J. Chem. Phys. 131, 124508 (2009).

435   - Trainoff, S.P., Cannell, D.S.: Physical optics treatment of the shadowgraph. Phys. of

436   Fluids 14, 1340-1363 (2002).

437   - Touzet, M., Galliero, G., Lazzeri, V., Saghir, M.Z., Montel, F., Legros, J.C.:

438   Thermodiffusion: from microgravity experiments to the initial state of petroleum

439   reservoirs, Comptes Rendus - Mécanique 339, 318-323 (2011).

440   - VanVaerenbergh, S., Srinivasan S., Saghir, M.Z.: Thermodiffusion in multicomponent

441   hydrocarbon mixtures: Experimental investigations and computational analysis. J.

442   Chem. Phys. 131, 114505 (2009).

443   - Wu, M., Ahlers, G., Cannell, D.S.: Thermally induced fluctuations below the onset of

444   the Rayleigh-Bénard convection. Phys. Rev. Lett. 75, 17432-1746 (1995).

445